

₁ Study of neutrino-nucleus interaction at around 1 GeV using
₂ cuboid lattice neutrino detector, WAGASCI, muon range
₃ detectors and magnetized spectrometer, Baby MIND, at
₄ J-PARC neutrino monitor hall

₅ A. Bonnemaison, R. Cornat, L. Domine, O. Drapier, O. Ferreira, F. Gastaldi,
₆ M. Gonin, J. Imber, M. Licciardi, F. Magniette, T. Mueller, L. Vignoli, and O. Volcy
₇ *Ecole Polytechnique, IN2P3-CNRS, Laboratoire Leprince-Ringuet, Palaiseau,*
₈ *France*

₉ S. Cao and T. Kobayashi

₁₀ *High Energy Accelerator Research Organization (KEK), Tsukuba, Ibaraki, Japan*

₁₁ M. Khabibullin, A. Khotjantsev, A. Kostin, Y. Kudenko, A. Mefodiev, O. Mineev,
₁₂ S. Suvorov, and N. Yershov

₁₃ *Institute for Nuclear Research of the Russian Academy of Sciences, Moscow, Russia*

₁₄ B. Quilain

₁₅ *Kavli Institute for the Physics and Mathematics of the Universe (WPI), The*
₁₆ *University of Tokyo Institutes for Advanced Study, University of Tokyo, Kashiwa,*
₁₇ *Chiba, Japan*

₁₈ T. Hayashino, A. Hiramoto, A.K. Ichikawa, K. Nakamura, T. Nakaya, K Yasutome,
₁₉ and K. Yoshida

₂₀ *Kyoto University, Department of Physics, Kyoto, Japan*

₂₁ Y. Azuma, J. Harada, T. Inoue, K. Kin, N. Kukita, S. Tanaka, Y. Seiya,
₂₂ K. Wakamatsu, and K. Yamamoto

₂₃ *Osaka City University, Department of Physics, Osaka, Japan*

24 A. Blondel, F. Cadoux, Y. Favere, E. Noah, L. Nicola, and S. Parsa

25 *University of Geneva, Section de Physique, DPNC, Geneva, Switzerland*

26 N. Chikuma, F. Hosomi, T. Koga, R. Tamura, and M. Yokoyama

27 *University of Tokyo, Department of Physics, Tokyo, Japan*

28 Y. Hayato

29 *University of Tokyo, Institute for Cosmic Ray Research, Kamioka Observatory,
30 Kamioka, Japan*

31 Y. Asada, K. Matsushita, A. Minamino, K. Okamoto, and D. Yamaguchi

32 *Yokohama National University, Faculty of Engineering, Yokohama, Japan*

33 December 15, 2017

34 **Abstract**

35 We, the WAGASCI collaboration, proposes to perform a study of neutrino-nucleus
36 interactions on the B2 floor of the neutrino monitor building with a new-type fine-
37 grained neutrino detector and muon range detectors. The hollow cuboid lattice scin-
38 tillators filled with water as the neutrino interaction target (known as WAGASCI
39 module) would enable the measurement of cross section on H₂O. Measurement in wide
40 phase space becomes possible by the combination of the WAGASCI modules, side- and
41 downstream- muon range detectors (MRD's). The downstream-MRD, the so-called
42 Baby MIND detector, also works as a magnet and provides charge identification ca-
43 pability as well as magnetic momentum measurement for high energy muons. The
44 nominal experimental setup has two WAGASCI modules. Most of the detectors have
45 already been constructed and have been commissioned in the J-PARC T59 experiment
46 and the CERN neutrino platform. Therefore, the collaboration will be ready to collect
47 physics data by January 2019. The experiment can run parasitically with T2K, without
48 dedicated beam time. With one-year data taking (roughly 5×10^{20} POT) in neutrino-
49 mode and another one-year in antineutrino mode, expected numbers of charged-current
50 interaction event are 5,400 and 2,240 for one WAGASCI module respectively. We will
51 provide inclusive and exclusive differential cross sections of the charged current neu-
52 trino and antineutrino interactions with water and hydrocarbon with a slightly higher
53 neutrino energy than T2K ND280 with wider angler acceptance. By combining our
54 measurements with those from ND280, model-independent extraction of the cross sec-
55 tion for narrow energy spread becomes possible. These measurements would improve
56 the understanding of the neutrino-nucleus interaction at around 1 GeV and also con-
57 tribute to reducing one of the most significant uncertainties of the T2K experiment.

58 **Contents**

| | | | |
|----|----------|--|-----------|
| 59 | 1 | Introduction | 4 |
| 60 | 2 | Experimental Setup | 5 |
| 61 | 2.1 | WAGASCI modules | 5 |
| 62 | 2.1.1 | Detector | 5 |
| 63 | 2.1.2 | Electronics | 7 |
| 64 | 2.1.3 | Water system | 9 |
| 65 | 2.2 | INGRID Proton module | 10 |
| 66 | 2.3 | Baby MIND | 11 |
| 67 | 2.3.1 | Magnet modules | 12 |
| 68 | 2.3.2 | Scintillator modules | 13 |
| 69 | 2.3.3 | Electronics | 15 |
| 70 | 2.3.4 | Performance check | 16 |
| 71 | 2.4 | Side muon range detector | 17 |
| 72 | 3 | Physics goals | 19 |
| 73 | 3.1 | Expected number of events | 20 |
| 74 | 3.2 | Pseudo-monochromatic beam by using different off-axis fluxes | 20 |
| 75 | 3.3 | Extraction of Cross sections | 20 |
| 76 | 3.4 | Subjects to which WAGASCI can contribute | 22 |
| 77 | 4 | Status of J-PARC T59 experiment | 24 |
| 78 | 5 | MC studies | 26 |
| 79 | 5.1 | Simulation setup | 26 |
| 80 | 5.2 | Charged-current event selection | 27 |
| 81 | 5.3 | Standalone WAGASCI-module tracking performance | 30 |
| 82 | 5.3.1 | Expected performance of the water-in WAGASCI module | 31 |
| 83 | 5.3.2 | Expected performance of the water-out WAGASCI module | 33 |
| 84 | 6 | Schedule | 34 |
| 85 | 7 | Requests | 34 |
| 86 | 7.1 | Neutrino beam | 34 |
| 87 | 7.2 | Equipment request including power line | 35 |

88 **1 Introduction**

89 The understanding of neutrino-nucleus interactions in the 1 GeV energy region is critical
90 for the success of accelerator-based neutrino oscillation experiments such as the T2K exper-
91 iment. Complicated multi-body effects of nuclei render this understanding difficult. The
92 T2K near detectors have been measuring these and significant progress has been achieved.
93 However, the understanding is still limited. One of the big factors preventing a complete
94 understanding is the non-monochromatic neutrino beam spectrum. Measurements with
95 distinct but partially overlapping beam spectra would be a great benefit in resolving the
96 contribution from different neutrino energies. We, the WAGASCI collaboration, proposes
97 to study the neutrino-nucleus interaction at the B2 floor of the neutrino monitor build-
98 ing, where different neutrino spectra from the T2K off-axis near detector (ND280) can
99 be obtained due to the different off-axis position. Our experimental setup contains two
100 hollow cuboid lattice detectors filled with water as the neutrino interaction target (known
101 as WAGASCI modules), two side- and one downstream- muon range detectors(MRD's).
102 We will have two types of the WAGASCI modules, a water-in module and a water-out
103 module. The water-in WAGASCI module has water the hollow cuboid lattice, and the
104 water-out WAGASCI module doesn't have water inside the lattice. The hollow cuboid
105 lattice and side-MRD's allow a measurement of wider-angle scattering than ND280. High
106 water to scintillator material ratio enables the measurement of the neutrino interaction
107 with water, which is highly desired for the T2K experiment because it's far detector,
108 Super-Kamiokande, is composed of water. The MRD's consist of plastic scintillators and
109 iron plates. The downstream-MRD, so called the Baby MIND detector, also works as a
110 magnet and provides the charge identification capability as well as magnetic momentum
111 measurement for high energy muons. The charge identification is essentially important to
112 select antineutrino events in the antineutrino beam because contamination of the neutrino
113 events is as high as 30%. Most of the detectors have already been constructed. The WA-
114 GASCI modules have been commissioned as the J-PARC T59 experiment and the Baby
115 MIND detector was commissioned at the CERN neutrino platform. Therefore, the collabo-
116 ration will be ready to proceed to the physics data taking by January 2019. We will provide
117 the cross sections of the charged current neutrino and antineutrino interactions on water
118 with slightly higher neutrino energy than T2K ND280 with wide angler acceptance. The
119 requested beam time is one-year in neutrino-mode and another one-year in antineutrino
120 mode assuming that the POT for the fast extraction in each year is more than 5×10^{20} POT.
121 When combined with ND280 measurements, our measurement would greatly improve the
122 understanding of the neutrino interaction at around 1 GeV and contribute to reducing one
123 of the most significant uncertainties of the T2K experiment.

124 **2 Experimental Setup**

125 Figure 1 and 2 show a schematic view and a CAD drawing of the entire set of detectors.
126 Central neutrino target detectors consist of two WAGASCI modules and T2K INGRID
127 proton module. Inside the WAGASCI module, plastic scintillator bars are aligned as a
128 hollow cuboid lattice and spaces in the lattice are filled with water for a water-in WAGASCI
129 module. T2K INGRID proton module is a full active neutrino target detector which is
130 composed only with scintillator bars in its tracking region. The central detectors are
131 surrounded by two side- and one downstream- muon range detectors(MRD's) The MRD's
132 are used to select muon tracks from the charged-current (CC) interactions and to reject
133 short tracks caused by neutral particles that originate mainly from neutrino interactions in
134 material surrounding the central detector, like the walls of the detector hall, neutrons and
135 gammas, or neutral-current (NC) interactions. The muon momentum can be reconstructed
136 from its range inside the detector. The MRD's consist of plastic scintillators and iron plates.
137 The downstream-MRD, also known as the Baby MIND detector, additionally has a coil
138 wound around each of the iron plates so it may be magnetized. This provides the charge
139 selection capability.

140 For all detectors, scintillation light in the scintillator bar is collected and transported
141 to a photodetector with a wavelength shifting fiber (WLS fiber). The light is read out by
142 a photodetector, Multi-Pixel Photon Counter (MPPC), attached to one end of the WLS
143 fiber. The signal from the MPPC is read out by the dedicated electronics developed for
144 the test experiment to enable bunch separation in the beam spill. The readout electronics
145 are triggered using the beam-timing signal from MR to synchronize to the beam. The
146 beam-timing signal is branched from those for T2K, and will not effect T2K data taking.

147 T2K adopted the off-axis beam method, in which the neutrino beam is intentionally
148 directed 2.5 degrees away from SK producing a narrow band ν_μ beam. The off-axis near
149 detector, ND280, is installed towards the SK direction in the B1 floor of the near detector
150 hall of the J-PARC neutrino beam-line. We propose to install our detector in the B2 floor
151 of the near detector hall, where the off-axis angle of 1.5 degrees is slightly different to the
152 2.5 degrees of ND280. The candidate detector position in the B2 floor is shown in Figure
153 3. The expected neutrino energy spectrum at the candidate position is shown in Figure 4.

154 **2.1 WAGASCI modules**

155 **2.1.1 Detector**

156 The WAGASCI modules are mainly composed of 1280 plastic scintillator bars and a sur-
157 rounding stainless steel tank as shown in Figure 5. The total number of channels in one
158 WAGASCI module is 1280. The stainless steel tank is constructed by welding stainless
159 steel plates, is sized as 460mm×1250mm×1250 mm, and weighs 0.5 tonne.

160 One WAGASCI module consists of 16 scintillator tracking planes, where each plane
161 is an array of 80 scintillator bars fixed with ABS frames. The 40 bars, called parallel

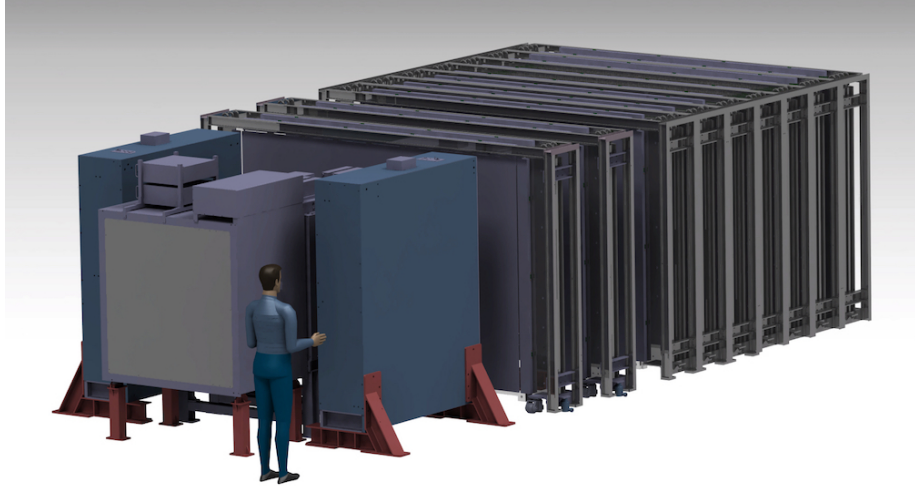


Figure 1: Schematic view of entire sets of detectors.

162 scintillators, are placed perpendicularly to the beam, and the other 40 bars, called lattice
 163 scintillators, are placed in parallel to the beam with hollow cuboid lattice in the tracking
 164 plane as shown in Figure 5. Thanks to the hollow cuboid lattice of the scintillator bars,
 165 the WAGASCI module has 4π angular acceptance for charged particles.

166 Thin plastic scintillator bars produced at Fermilab by extrusion method, mainly consists
 167 of polystyrene and are surrounded by thin reflector including TiO^2 (3 mm in thickness)
 168 are used for the WAGASCI modules to reduce the mass ratio of scintillator bars to water,
 169 because neutrino interactions in the scintillator bars are a background for the cross section
 170 measurements on H_2O . Each scintillator bar is sized as 1020mm \times 25mm \times 3 mm including
 171 the reflector part, and half of all the scintillator bars have 50-mm-interval slits to form the
 172 hollow cuboid lattice (Figure 6).

173 We will have two types of the WAGASCI modules, a water-in module and a water-out
 174 module. The water-in WAGASCI module has water in spaces of the hollow cuboid lattice.
 175 The total water mass serving as neutrino targets in the fiducial volume of the module is
 176 188 kg, and the mass ratio of scintillator bars to water is 80 %. The water-out WAGASCI
 177 module doesn't have water inside the detector. The total CH mass serving as neutrino
 178 target in the fiducial volume of the module is 47 kg, and the mass fraction of scintillator
 179 bars is 100 %.

180 Scintillation light is collected by wave length shifting fibers, Y-11 (non-S type with a
 181 diameter of 1.0 mm produced by Kuraray. A fiber is glued by optical cement in a groove
 182 on surface of a scintillator bar. 32 fibers are gathered together by a fiber bundle at edge
 183 of the module, and lead scintillation light to a 32-channel arrayed MPPC. Since crosstalk

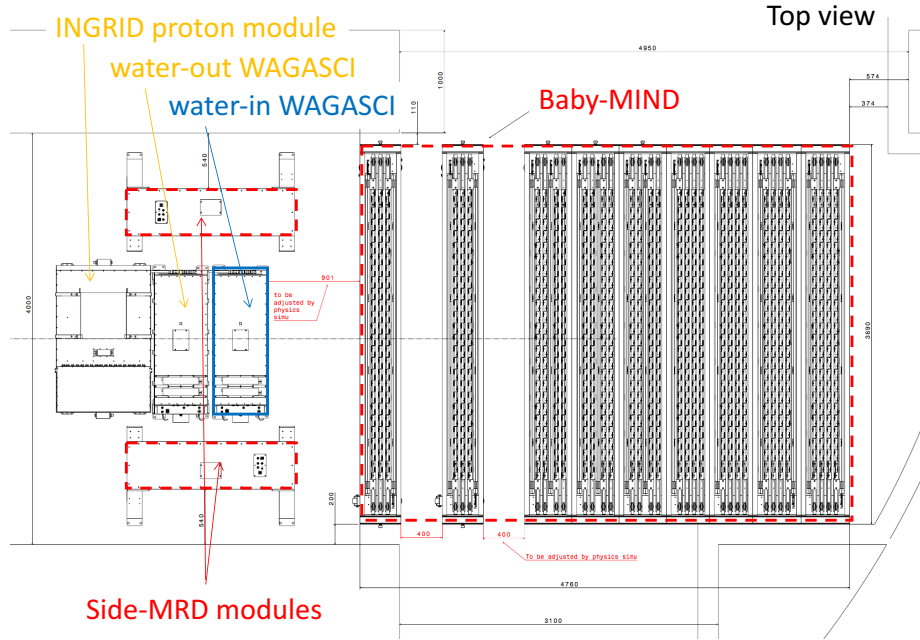


Figure 2: Top view of entire sets of detectors.

of light yield due to reflection on the inner surface of each cell has been observed, all the scintillator bars are painted black by aqueous color spray. It is confirmed by measurements with cosmic rays that black painting on the surface of the scintillator bars suppresses this crosstalk so that no significant crosstalk effect is observed within uncertainty.

32-channel arrayed MPPCs, as shown in the Figure 7, are used for the modules. The surface of the fiber bundle is polished and directly attached onto the 32-channel arrayed MPPCs. The positions of 32 fibers on the bundle are aligned to fit the channels of MPPCs. The MPPC is a product of Hamamatsu Photonics, S13660(ES1), with suppressed noise rate of \sim 6 kHz per channel at 0.5 p.e. threshold. For each MPPC channel, 716 pixels of APD are aligned in a shape of circle.

194 2.1.2 Electronics

195 As front-end electronics of this detector, a Silicon PM Integrated Read-Out Chip (SPIROC)
 196 [13] is adopted. SPIROC is a 36-channel auto-triggered front-end ASIC, and is produced
 197 by OMEGA/ IN2P3. It not only contains an analog signal processing part such as amplifi-
 198 cation and shaping of the waveform, but contains a digital signal processing parts such as
 199 auto-trigger and timing measurement. Charge of MPPC signal is sampled by track-and-

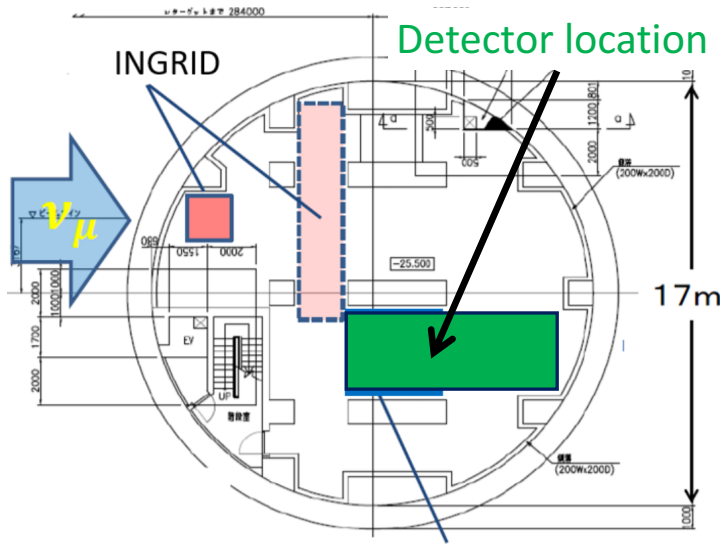


Figure 3: Candidate detector position on the B2 floor of the near detector hall.

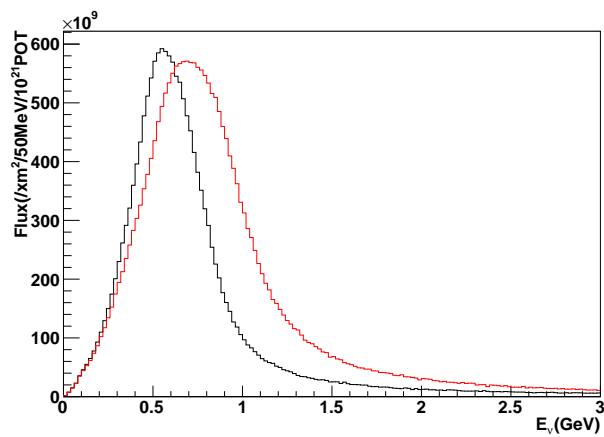


Figure 4: Neutrino energy spectrum at the candidate detector position (red, off-axis 1.5 degree). The spectrum at the ND280 site (black, off-axis 2.5 degree) is also shown.

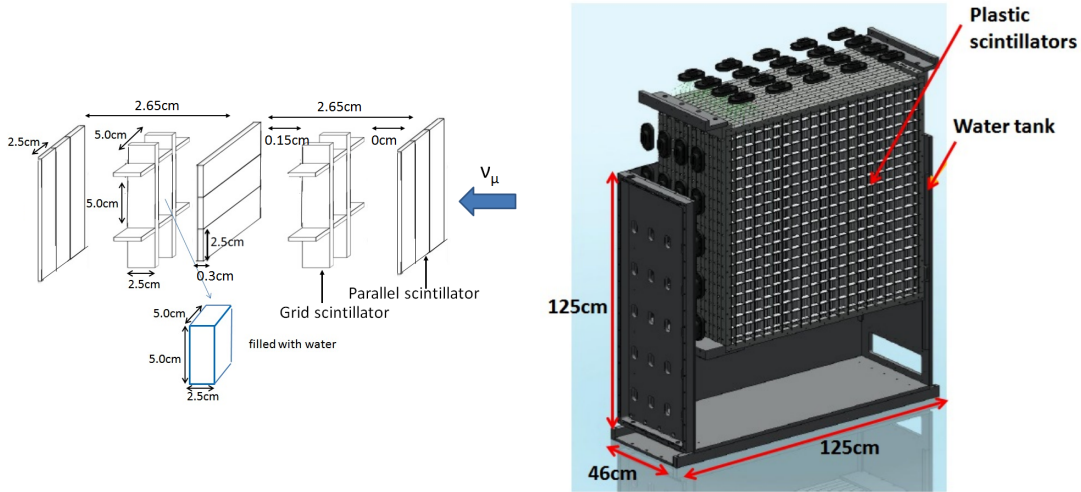


Figure 5: Schematic views of hollow cuboid lattice of plastic scintillator bars (left) and WAGASCI module (right).

hold circuit. A Front-end electronics board, Active Sensor Unit (ASU), has been developed with the SPIROC2D chip, which is the latest version of SPIROC. Each readout board is designed to control a 32-channel arrayed MPPC, and 40 of the ASU boards are aligned on the module surface. The data acquisition system used for this detector, including back-end boards, has been developed for prototypes of ultra-granular calorimeters for the International Linear Collider (ILC) [6], and independent of the T2K DAQ system. To synchronize the DAQ system to J- PARC neutrino beam, pre-beam trigger and beam trigger are sent to the clock control card. The beam trigger signals are converted from optical signals to NIM signals at NIM module on the B2 floor. In addition, the information of spill number are delivered with 16-bit ECL level signals, and converted to an Ethernet frame by an FPGA evaluation board to be directly sent to the DAQ PC. The electronics readout scheme is shown in Figure 8.

2.1.3 Water system

Pure water is filled to the water tank of the water-in WAGASCI module as follows. First, the water storage tank located at the B2 floor of the NM pit is filled with water delivered from a water tap on the ground level through a long hose. Second, the water is pumped to the other water storage tank though a water filler to produce pure water. Third, a compound preservative called Germall plus, which is the same preservative used in one of the sub-detectors of T2K ND280, FGD2, is put into the water to keep water from being bad. Then, the water is poured to the water-in WAGASCI module, and it is kept in the

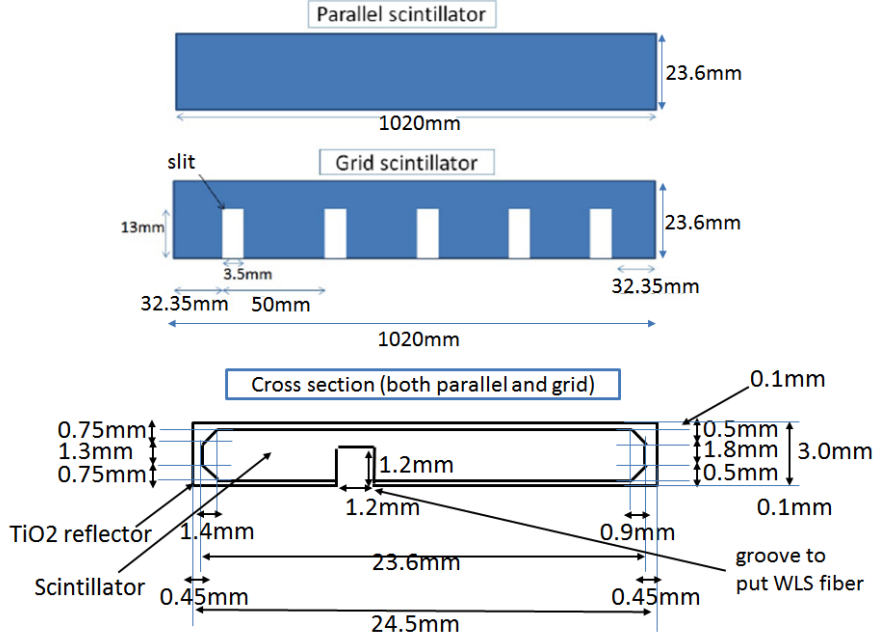


Figure 6: Geometry of scintillators used for WAGASCI modules.

220 module during the neutrino beam operation and not to be circulated.

221 2.2 INGRID Proton module

222 INGRID Proton module is a neutrino detector of the T2K experiment. It is a fully-active
 223 tracking detector which consists of only scintillator strips. The purpose of this Proton
 224 Module is to separate the neutrino interaction types by detecting the protons and pions
 225 together with the muons from the neutrino interactions, and to measure the neutrino cross
 226 section for each interaction type. It consists of 36 tracking planes surrounded by veto
 227 planes (Figure 9), where each tracking plane is an array of two types of scintillator strips.
 228 The 16 strips in the inner region have dimensions of $25\text{mm} \times 13\text{mm} \times 1200\text{mm}$, while the 16
 229 strips in the outer region have dimensions of $50\text{mm} \times 10\text{mm} \times 1200\text{mm}$, making a plane of
 230 $1200\text{mm} \times 1200\text{mm}$ in the horizontal and vertical directions. The former is the scintillator
 231 produced for the K2K SciBar detector [4] and the latter was produced for INGRID. The
 232 tracking planes are placed perpendicular to the beam axis at 23mm intervals. Since the
 233 strips are aligned in one direction, each tracking plane is sensitive to either the horizontal or
 234 vertical position of the tracks. The tracking planes are therefore placed alternating in the
 235 horizontal and vertical directions so that three-dimensional tracks can be reconstructed.
 236 The tracking planes also serve as the neutrino interaction target. As with the WAGASCI

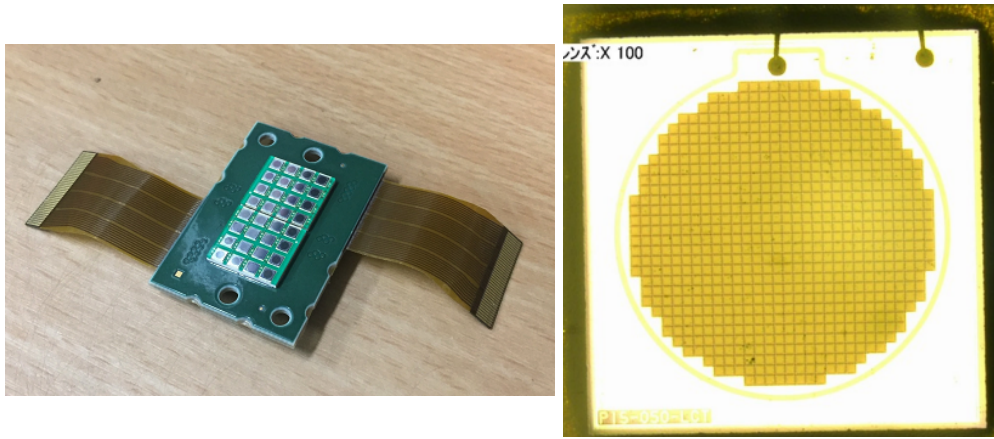


Figure 7: 32-channel arrayed MPPC (left) and an enlarged view of one MPPC channel (right).

237 modules, scintillation light is read out by a WLS fiber and MPPC.

238 It was installed on the neutrino beam axis on the SS floor of the T2K near detector hall
 239 in 2010, and had been used for neutrino cross section measurements. In August 2017, it
 240 was moved to the B2 floor of the T2K near detector hall by J-PARC T59 after getting the
 241 approval from T2K to use them. J-PARC T59 is performing a neutrino beam measurement
 242 using the detector from October 2017, and the measurement will continue until May 2018
 243 as we will discuss in Sec. 4.

244 We will operate the INGRID Proton module using the T2K near detector electronics/DAQ
 245 system in the same way as J-PARC T59. A proposal to use the module and its
 246 electronics for our project will be submitted to the T2K collaboration.

247 2.3 Baby MIND

248 The Baby MIND is the downstream Muon Range Detector. It also works as a magnet and
 249 provides the charge identification capability as well as magnetic momentum measurement
 250 for high energy muons.

251 The Baby MIND collaboration ¹ submitted a proposal to the SPSC at CERN, SPSC-P-
 252 353. The project was approved by the CERN research board as Neutrino Platform project
 253 NP05 and constructed. The detector consists of 33 magnet modules, each 3500 mm ×
 254 2000 mm × 50 mm (30 mm steel) with a mass of approximately 2 tonnes. Of these magnet
 255 modules, 18 are instrumented with plastic scintillator modules.

¹Contact person: E. Noah, Spokesperson: A. Blondel, Deputy spokesperson: Y. Kudenko

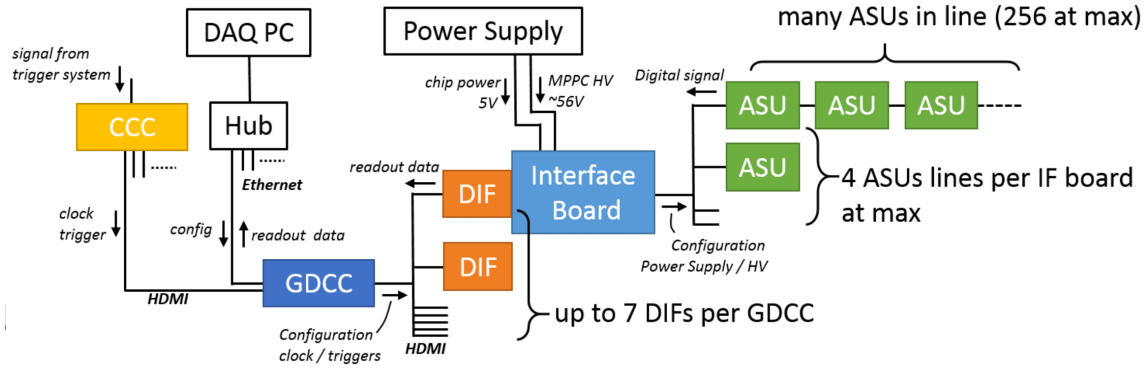


Figure 8: WAGASCI electronics readout scheme.

2.3.1 Magnet modules

Traditional layouts for magnetized iron neutrino detectors (e.g. MINOS) tend to be monolithic blocks with a unique pitch between consecutive steel segments and large conductor coils threaded around the whole magnet volume. The Baby MIND detector, like traditional designs, is built from sheets of iron interleaved with scintillator detector modules. However Baby MIND is novel in that the iron segments are all individually magnetized as shown in Figure 10, allowing for far greater flexibility in the setting of the pitch between segments, and in the allowable geometries that these detectors can take.

The key design outcome is a highly optimized magnetic field map. A double-slit configuration for coil winding was adopted to increase the area over which the magnetic flux lines are homogeneous in B_x across the central tracking region. Simulations show the magnet field map to be very uniform over this central tracking region covering an area of $2800 \times 2000 \text{ mm}^2$, Figure 11. The B_x component dominates in this region, with negligible B_y and B_z . This was confirmed by measuring the field with 9 pick-up coils wound around the first module. Subsequent modules were equipped with one pick-up coil. Test results on the 33 modules show all achieve the required field of 1.5 T for a current of 140 A, with a total power consumption of 11.5 kW. The polarity of the field map shown in Figure 11 (middle) can be reversed by changing the power supply configuration.

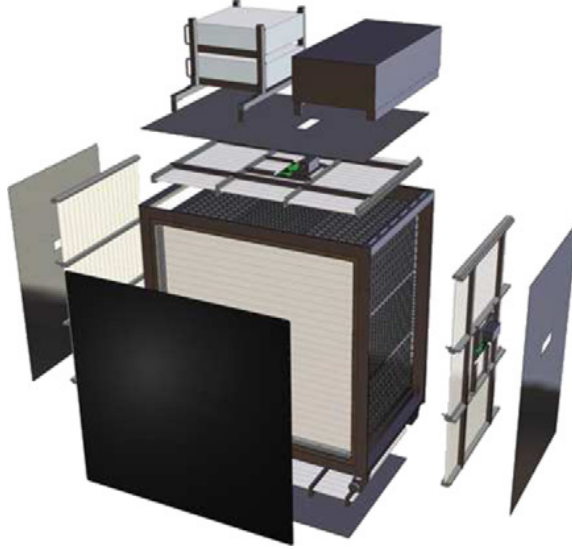


Figure 9: Schematic view of INGRID Proton module.

2.3.2 Scintillator modules

Each of the 18 scintillator modules is constructed from 2 planes of horizontal counters (95 counters in total) and 2 planes of vertical counters (16 counters in total) [3], arranged with an overlap between planes to achieve close to 100% hit efficiency for minimum ionizing muons. The arrangement of planes within a module is vertical-horizontal-horizontal-vertical. This arrangement was the result of an assembly approach whereby each plane was built from 2 half-planes, with each half plane consisting of a horizontal plane and a vertical plane. The scintillator bars are held in place using structural ladders that align and maintain the counters, Figure 12. No glue is used in the process, so counters can be replaced. Aluminum sheets front and back provide light tightness.

The plastic scintillator counters were made from 220 mm-wide slabs, consisting of extruded polystyrene doped with 1.5% paraterphenyl (PTP) and 0.01% POPOP. They were cut to size then covered with a 30-100 μm thick diffuse reflector resulting from etching of the surface with a chemical agent [10, 11]. The horizontal counter size is $2880 \times 31 \times 7.5 \text{ mm}^3$, with one groove along the length of the bar in which sits a wavelength shifting fiber from Kuraray. The vertical counter size is $1950 \times 210 \times 7.5 \text{ mm}^3$, with one U-shaped groove along the bar. On each counter, two custom connectors house silicon photomultipliers, MPPC type S12571-025C from Hamamatsu, either side of the horizontal counter, and both connectors at the top for the vertical counter. This geometrical configuration for vertical counters was chosen for ease of connectivity to the electronics, and maintenance operations.

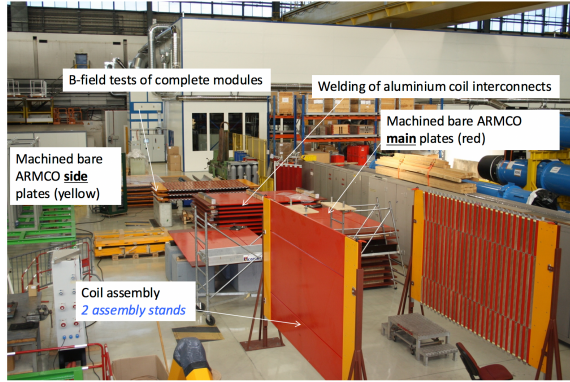


Figure 10: Magnet assembly zone at CERN.

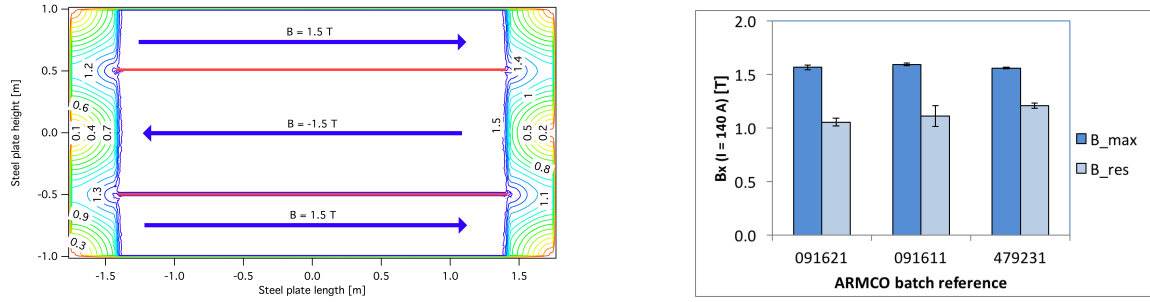


Figure 11: Left) Magnetic field map with a coil along 2800 mm of the length of the plate. Right) Measured B field for 33 modules.



Figure 12: Scintillator modules assembly. Left) top of front half-module showing vertical counters, and the spacer-ladders that set the pitch between horizontal counters and hold them in place. Middle) rear half-module showing horizontal counters on their ladders. Right) Assembled rear half-module, the front half-module can be seen in the background.

295 A total of 1744 horizontal counters and 315 vertical counters (including spares) were
 296 produced at the Uniplast company (Vladimir, Russia).

297 2.3.3 Electronics

298 The Baby MIND electronic readout scheme includes several custom-designed boards [12].
 299 The revised version is shown in Figure 13. At the heart of the system is the electronics
 300 Front End Board (FEB), developed by the University of Geneva. The readout system
 301 includes two ancillary boards, the Backplane, and the Master Clock Board (MCB) whose
 302 development has been managed by INRNE (Bulgarian Academy of Sciences) collaborators.

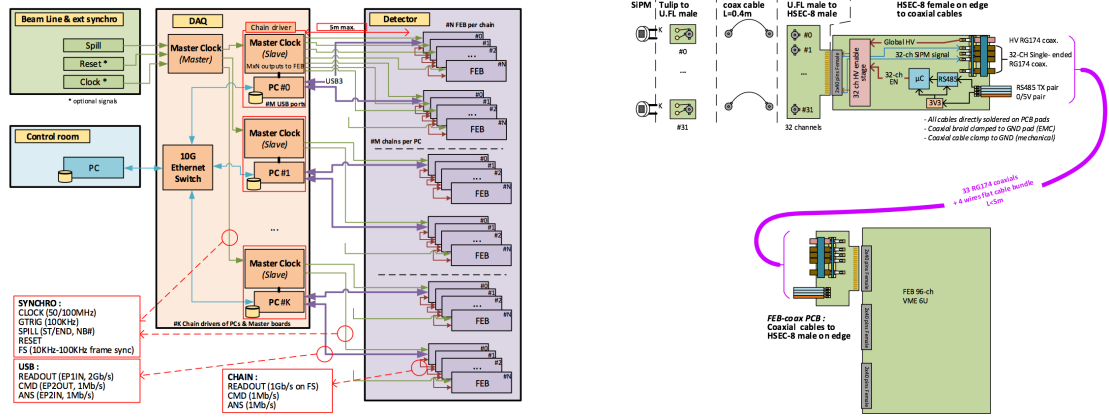


Figure 13: Left) Baby MIND electronics readout scheme. Right) SiPM-to-FEB connectivity.

303 The FEBv2 hosts 3 CITIROC chips that can each read in signals from 32 SiPMs [7].
 304 Each signal input is processed by a high gain (HG), and a separate low gain (LG), signal
 305 path. The outputs from the slow shapers can be sampled using one of two modes: a
 306 mode with an externally applied delay, and a peak detector mode. A faster shaper can be
 307 switched to either HG or LG paths, followed by discriminators with adjustable thresholds
 308 providing 32 individual trigger outputs and one OR32 trigger output. An Altera ARIA5
 309 FPGA on the FEBv2 samples these trigger outputs at 400 MHz, recording rising and falling
 310 times for the individual triggers and assigning time stamps to these. Time-over-threshold,
 311 the difference between falling and rising times, gives some measure of signal amplitude.
 312 This is used in addition to charge information and proves useful if there is more than
 313 one hit per bar within the $\sim 9 \mu\text{s}$ deadtime due to the readout of the multiplexed charge
 314 output. The ARIA5 also manages the digitization of the sampled CITIROC multiplexed
 315 HG and LG outputs via a 12-bit 8-ch ADC.

316 The internal 400 MHz clock on the FEBv2 can be synchronized to a common 100 MHz
 317 clock. The synchronization subsystem combines input signals from the beam line into

318 a digital synchronization signal (SYNC) and produces a common detector clock (CLK)
 319 which can eventually be synchronised to an external experiment clock. Both SYNC and
 320 CLK signals are distributed to the FEBs. Tests show the FEB-to-FEB CLK(SYNC) delay
 321 difference to be 50 ps (70 ps). Signals from the beam line at WAGASCI include two
 322 separate timing signals, arriving 100 ms and 30 μ s before the neutrino beam at the near
 323 detectors. The spill number is available as a 16-bit signal.

324 2.3.4 Performance check

325 All counters were measured at INR Moscow with a cosmic ray setup using the same type
 326 S12571-025C MPPCs and a CAEN DT5742 digitizer. The average light yield (sum from
 327 both ends) was measured to be 37.5 photo-electrons (p.e.) per minimum ionizing particle
 328 (MIP) and 65 p.e./MIP for vertical and horizontal counters, respectively. After shipment
 329 to CERN, all counters were individually re-tested with an LED [?]. 0.1% of counters failed
 330 the LED tests and were therefore not used during the assembly of modules. The assembly
 331 of modules was completed in June 2017, and it was then tested in June and July 2017 at
 332 the Proton Synchrotron experimental hall at CERN with a mixed particle beam comprising
 333 mostly muons whose momenta could be selected between 0.5 and 5 GeV/c. Muon tracks
 334 from the summer 2017 beam tests are shown in Figure 14 for different muon momentum
 beam settings and for both muon polarities.

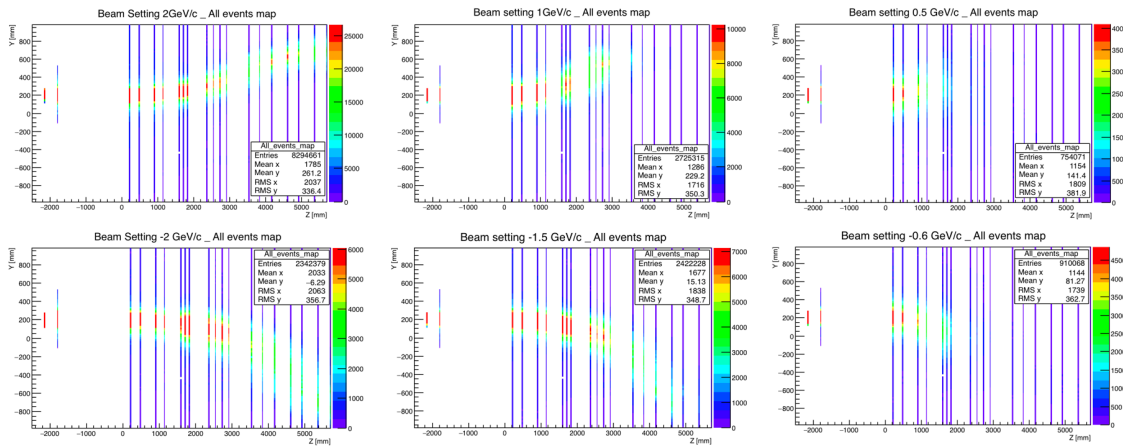


Figure 14: Y-Z hit profiles in Baby MIND detector modules for positive (upper row) and negative (lower row) muon beam settings during the summer 2017 beam tests at the CERN-PS facility. Muon momentum settings for the beam shown here are 2 GeV/c, 1.5 GeV/c and 0.5 GeV/c for left, middle and right plots respectively.

335

336 **2.4 Side muon range detector**

337 Two Side-MRD modules for tracking secondary particles from neutrino interactions will be
338 installed in 2018. Each Side-MRD module is composed of 11 steel plates and 80 scintillator
339 slabs. The slabs are arranged as 10 layers installed in the 13 mm gaps between the 30 mm
340 thick plates. Each steel plate size is 30 mm \times 1610 mm \times 1800 mm. Total module size is
341 2236 mm \times 1630 mm \times 975 mm as shown in Figure 15 (left), weight is \sim 8.5 tonne.

342 Scintillator bars were manufactured by Uniplast company in Vladimir, Russia. Polystyrene
343 based scintillators were extruded with thickness of 7 mm, then cut to the size of 7 \times 200 \times
344 1800 mm³. Dopant composition is 1.5% PTP and 0.01% POPOP. Scintillator surface was
345 etched by a chemical agent to form a white diffuse layer with excellent reflective perfor-
346 mance. Ideal contact between the scintillator and the reflector raises the light yield up
347 to 50% comparing to an uncovered scintillator. A sinusoidal groove was milled along the
348 scintillator to provide uniform light collection over the whole scintillator surface. WLS Y11
349 Kuraray fiber of 1 mm diameter was glued with an optical cement EJ-500 in the S-shape
350 groove as shown in Figure 15(right). A minimum bending radius of 30 mm was used to
351 ensure the the Kuraray S-type fibers remained within specification. Both ends of the fiber
352 were glued into optical connectors which were themselves attached to the scintillator and
353 provide an interface to SiPMs, Hamamatsu MPPC S13081-050CS(X1).

354 Scintillators for the Side-MRD modules were assembled at INR in Russia, and shipped
355 to Japan in July 2017. The light yield for each scintillator was measured with cosmic
356 rays at INR and at YNU in Japan after delivery. LY_1 and LY_2 are light yields measured
357 at both ends of the counter. The light yield asymmetry between the ends calculated as
358 $100\% \times \frac{LY_1 - LY_2}{LY_1 + LY_2}$. After tests at INR we selected 324 counters from measured 332 ones with
359 the mean light yield of 45 p.e./MIP ($LY_1 + LY_2$) and the asymmetry value less than 10
360 %. The measurements at YNU yielded the average total light yield of about 40 p.e./MIP
361 which varies in range from 32 to 50 p.e./MIP (Figure 16 (left)). Only two counters showed
362 relatively high asymmetry close to 25 % as shown in Figure 16 (right). Using the results of
363 the quality assurance test we selected 320 scintillator counters for the Side-MRD modules.

364 We also measured the time resolution for a combination of four counters piled one
365 upon another. The average result for four counters is $\sigma_T = 1.04$ ns. The resolution of
366 combination of 2, 3, 4 counters is measured to be 0.79 ns, 0.66 ns and 0.58 ns, respectively.

367
368 Construction of the Side-MRD modules is scheduled from November 2017 at Yokohama
369 National University. They will then be transported to J-PARC for installation on the B2
370 floor of the T2K near detector hall.

371 Same electronics as the WAGASCI modules (see Sec. 2.1.2) are used for the Side-MRD
372 modules.

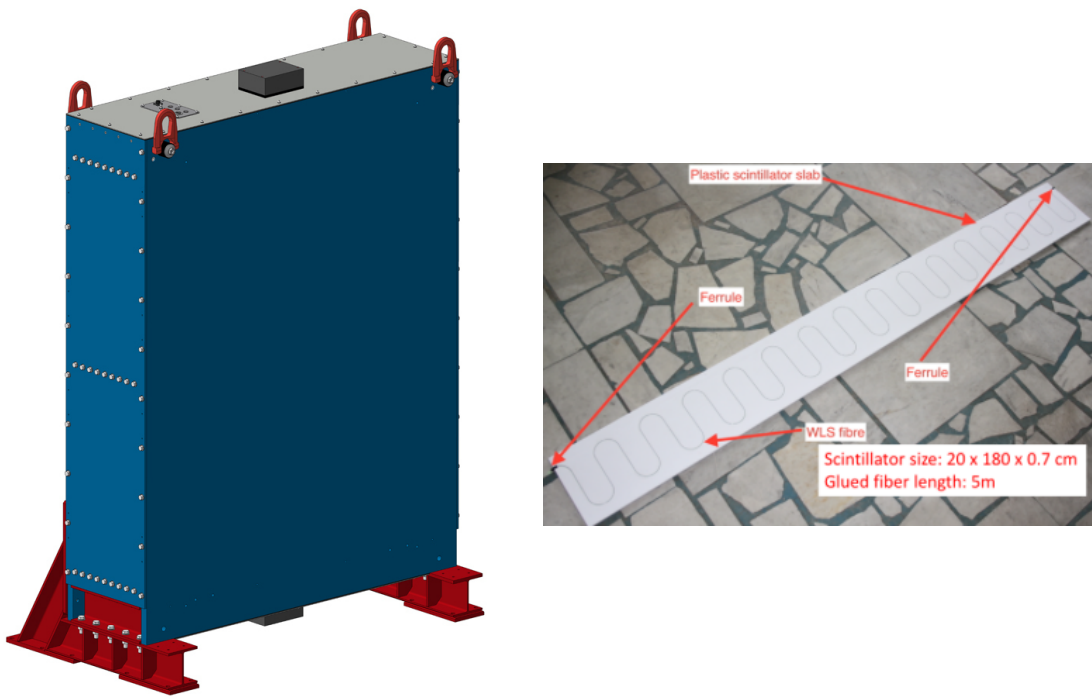


Figure 15: Left :Side-MRD module. Right: Scintillator bar of the Side-MRD modules.

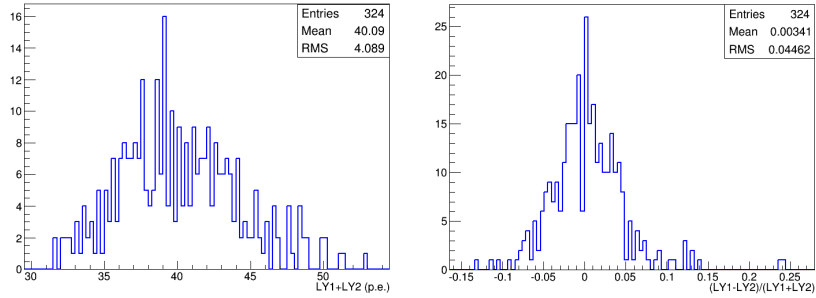


Figure 16: Total light yield distribution (left) and light yield assymetry (right) measured at YNU.

3 Physics goals

We will measure the differential cross section for the charged-current (CC) interaction on H₂O and Hydrocarbon(CH). The water-scintillator mass ratio of the WAGASCI module is as high as 4:1 and the high purity measurement of the cross section on H₂O is possible. One experimental option is to remove water from one of the two WAGASCI modules. The water-out WAGASCI module will allow to measure pure-CH target interactions with very low momentum-threshold for protons. This will also allow this CH interaction background to be subtracted from the water-in target measurement. Another option is to add the T2K proton module which is fully made of plastic scintillators. It will allow a high statistics comparison of cross section between H₂O and CH and also comparison with ND280 measurements. The actual configuration will be optimized with detailed MC simulation by 2018 Summer.

Our setup allows the measurements of inclusive and also exclusive channels such as 1 μ , 1 μ 1p, 1 μ 1 π^{\pm} np samples, the first two of which are mainly caused by the quasi-elastic and 2p2h interaction and the latter is mainly caused by resonant or coherent pion production and deep elastic scattering. In general, an accelerator produced neutrino beam spectrum is wide and the energy reconstruction depends upon the neutrino interaction model. Therefore, recent neutrino cross section measurements including those from T2K are given as a flux-integrated cross section rather than cross sections as a function of the neutrino energy to avoid model dependence. We can provide the flux-integrated cross section. In addition, by combining our measurements with those from ND280, model-independent extraction of the cross section for narrow energy spread becomes possible. This method was demonstrated in [1] and also proposed by E61 (NUPRISM) experiment.

395 **3.1 Expected number of events**

396 The expected number of CC neutrino events remaining after the event selections was eval-
397 uated with simulation. Details are described in Sec. 5. In neutrino-mode, 5,400, 1,100
398 and 3,800 events are expected for the water-in WAGASCI module, the water-out WA-
399 GASCI module and the INGRID proton module, respectively, with 5×10^{20} POT. Among
400 5,400 events for the water-in WAGASCI module, 78 % are interactions on H₂O. In the
401 antineutrino-mode, 2,240, 400 and 1,500 CC antineutrino events are expected for the water-
402 in WAGASCI module, the water-out WAGASCI module and the INGRID proton module,
403 respectively, with 5×10^{20} POT. Among the 2,240 events observed in the water-in WAGSCI
404 module, 74% are interactions on H₂O. The wrong-sign interactions in antineutrino-mode
405 is 561 events, but will be removed with 90 % or higher efficiency by Baby MIND.

406 **3.2 Pseudo-monochromatic beam by using different off-axis fluxes**

407 The off-axis method gives narrower neutrino spectrum, and the peak energy is lower for
408 larger off-axis angle. There still remains a high energy tail mainly due to neutrinos from
409 Kaon decay. The off-axis angle of the WAGASCI location is 1.5 degrees as opposed to 2.5
410 degrees for ND280. The top two plots of Figure 17 show the energy spectra of fluxes and
411 neutrino interactions at these two different locations. The Bottom two plots of Figure 17
412 show the energy spectra of fluxes and neutrino interaction events obtained by subtraction
413 of fluxes at ND280 and WAGASCI. We can effectively get two fluxes, from 0.2 GeV to
414 0.9 GeV and 0.6 GeV and 2 GeV and measure flux-integrated cross section for these two
415 fluxes. It should be noted that even though the statistical errors are drawn for each energy
416 bin for the bottom right plot of Fig. 17, measurement results will be given as an integration
417 across energies.

418 **3.3 Extraction of Cross sections**

The flux-integrated CC inclusive cross sections on H₂O and CH are calculated from the
number of selected events with background subtraction and efficiency correction

$$\sigma_{CC} = \frac{N_{sel} - N_{BG}}{\phi T \epsilon},$$

419 where N_{sel} is the number of selected events from the real data, N_{BG} is the number of
420 background events contaminating the selected sample, ϕ is the integrated ν_μ flux, T is the
421 number of target nucleons, and ϵ is the detection efficiency for signal estimated by MC sim-
422 ulation. The number of main background events is estimated from sideband samples. The
423 CH interaction background for the H₂O measurement is estimated from the measurement
424 of the Water-out WAGASCI module and/or the proton module. The neutrino interaction
425 background for the antineutrino measurement is estimated from the opposite-sign inter-
426 actions selected by Baby MIND. The dominant error for the inclusive total cross section

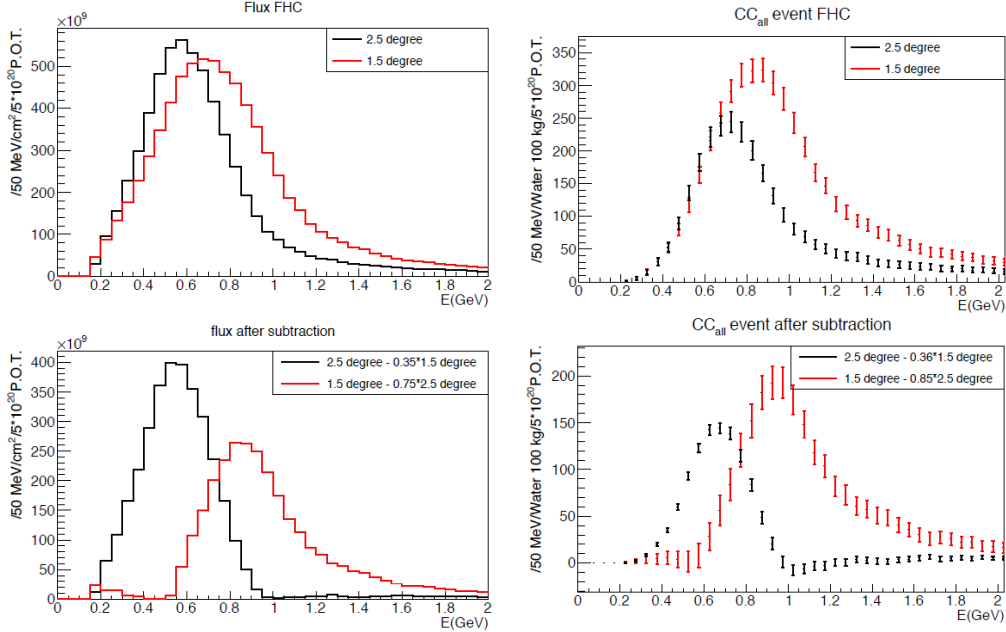


Figure 17: Energy spectra obtained by using different off-axis angle fluxes. Top two plots show the energy distribution of the fluxes (left) and interactions (right) for ND280 (off-axis 2.5 degree) and WAGASCI (off-axis 1.5 degree). Bottom two plots show the fluxes (left) and spectra of interaction events (right) obtained by subtraction of fluxes at ND280 and WAGASCI. The error bars represent the statistical error and those in the bottom right plot assume the statistical error for ND280 measurements are much smaller than those of the WAGASCI experiment.

measurement is the uncertainty of the neutrino flux, which is $\sim 9\%$ now and is expected to be reduced to $\sim 6\%$. Since the flux error is dominated by normalization uncertainties that are correlated across measurements on the different target materials and locations, the flux error can be significantly reduced for the relative comparison of the H₂O and CH cross sections and the relative comparison of the ND280 and WAGASCI measurements. For example, T2K INGRID succeeded to determine the cross section ratio for CH and Fe with 3% precision[5]. For the exclusive and/or differential cross section measurements, statistical error would be dominant, the size of which depends on the binning.

3.4 Subjects to which WAGASCI can contribute

Recent accelerator neutrino experiments use nuclear target e.g. organic scintillator, water and iron. So the interactions are significantly affected by nuclear effects such as Fermi motion, correlated pairs of nucleons in nucleus (two particles-two holes, 2p2h), collective nuclear effects and final state interactions (FSI) of secondary particles in the nuclei after the initial neutrino interactions.

The main interaction type at the T2K energy (sub GeV) is the CC quasi-elastic (CCQE) interaction with nucleons inside nucleus. The energy is reconstructed from the lepton momentum assuming CCQE kinematics in T2K, which is biased in the case of other interaction channels. Figure 18 shows how the reconstructed energy is affected. The 2p2h interactions mainly happen through the interaction with a correlated nucleons pair and also through the Δ resonance interaction followed by pion-less decay. The 2p2h interactions are observed in electron scattering experiments [8] where the 2p2h events were observed in the gap between the quasi-elastic and pion-production regions. Neutrino experiments have attempted to measure the 2p2h interactions, but so far there are only indicative results. This is because the transferred momentum (p) and energy (ω) cannot be determined in the neutrino experiments due to the wide energy spectrum of the neutrino beam. Our measurements, when combined with ND280 measurement, will give the cross section values for narrow energy-spread fluxes and give insight for such interactions. Another efficient way to investigate the 2p2h interaction is direct measurement of proton tracks with low momentum threshold and wide acceptance. Figure 19 left plot shows proton multiplicities for the CCQE events and 2p2h events. Figure 19 right plot shows the opening angles between the protons in events with two outgoing protons. The water-out WAGASCI can provide good sample for the 2p2h interaction search because its low density medium enables the detection of low momentum protons at wide angles.

There are various models which describe the collective nuclear effects [9]. The wide acceptance of the WAGASCI experiment will provide information complementary to ND280 and will play an important role to select and tune models.

T2K is starting to use ν_e CC1 π samples at the far detector to increase statistics. One of the biggest uncertainty of the CC1 π sample comes from the final state interactions of pions in the nuclei after the initial neutrino interactions because they change the multi-

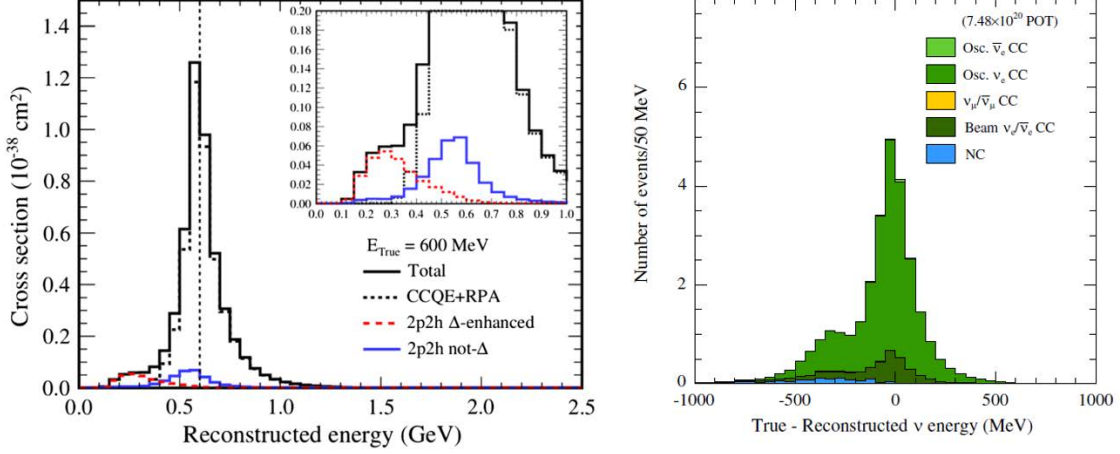


Figure 18: Left: reconstructed neutrino energy for CCQE and 2p2h interactions of simulated 600 MeV muon neutrinos on ^{12}C . Right: difference between true and reconstructed energy of the ν_e CCQE-like sample. The energy is reconstructed from the lepton momentum assuming the kinematics of the CCQE interaction. Both plots from [2]

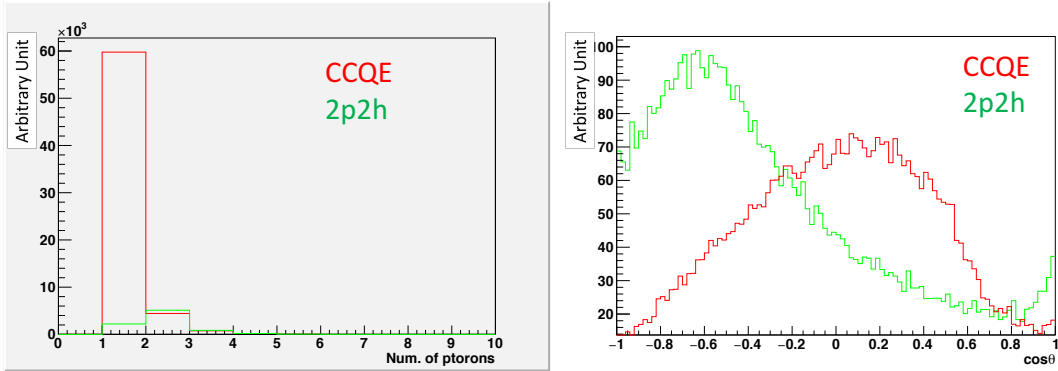


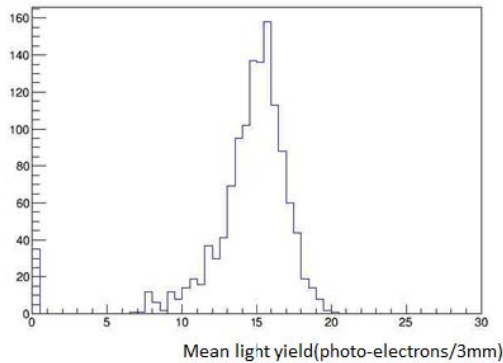
Figure 19: Proton multiplicities (left) and opening angles between two proton tracks (right) for CCQE events and 2p2h events. The final-state interaction is taking into account.

466 plicity, charge and kinematics of the pions. Multi pion production events can migrate into
467 the CC1pi sample due to FSI and become background. The WAGASCI module has the
468 capability to distinguish the pion track and proton track by dE/dx , so WAGASCI can
469 provide the $CC1\pi$ cross section with low momentum threshold and wide acceptance for
470 pion tracks.

471 4 Status of J-PARC T59 experiment

472 We had submitted a proposal of a test experiment to J-PARC in April 2014 to test a new
473 detector with a water target, WAGASCI, at the neutrino monitor hall, and the proposal
474 was approved as J-PARC T59. The project contains the side and downstream muon range
475 detectors as well.

476 The first WAGASCI module has been constructed in 2016 and installed at the on-axis
477 position in front of the T2K INGRID detector for the commissioning and the first cross
478 section measurement as a part of the T2K experiment. The INGRID electronics boards are
479 used to read the signal. The light yield measured with muons produced by the interaction
480 of neutrinos in the hall wall, shown in Figure 20, is sufficiently high to get a good hit
efficiency. A track search algorithm based on the cellular automaton has been developed



481
482
483
484
485
486
487 Figure 20: Light yield for muons produced by the interaction of neutrinos in the hall wall.
Average light yields for each channel are plotted.

481 using the software tools from T2K INGRID. Examples of observed events are shown in
482 Figure 21. The tracking efficiency in a 2-dimensional projected plane was evaluated by
483 comparing the reconstructed track in the WAGASCI module and the INGRID module,
484 and is shown in Figure 22. Note that that the tracking efficiency for high angle (> 70 deg)
485 is not evaluated because of the acceptance of the INGRID module, not because of the
486 limitation of the WAGASCI module.

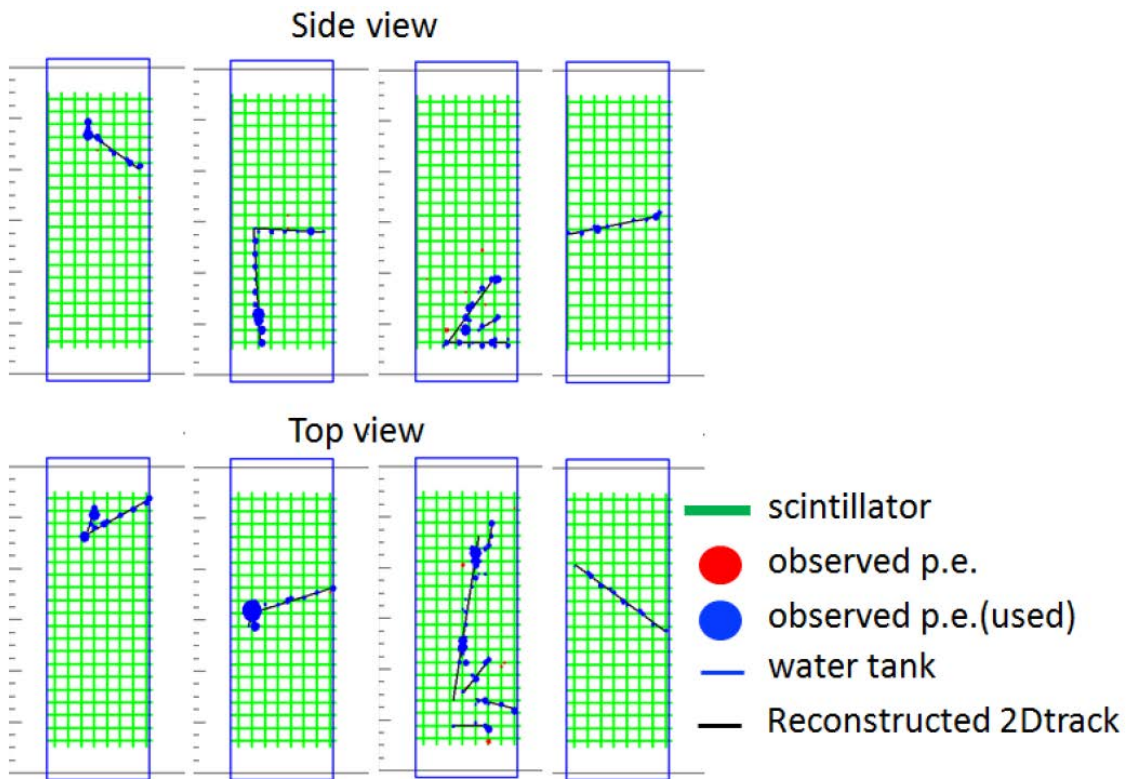


Figure 21: Example event displays of the WAGASCI module at on-axis. The reconstructed tracks are overlaid.

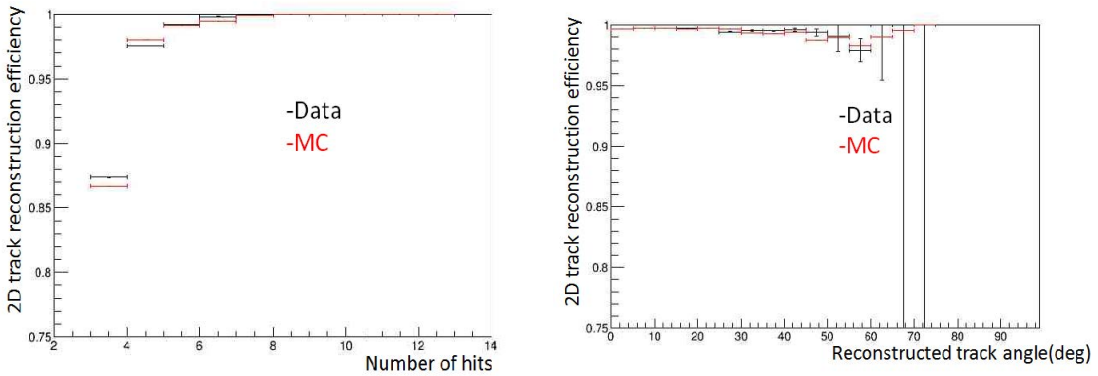


Figure 22: 2D track reconstruction efficiency as a function of number of hits (left) and track angle (right). Here the track angle is the one reconstructed by the INGRID module.

488 In 2017 Autumn, the construction of the second WAGASCI module and the dedicated
 489 electronics board were completed. The module and the electronics were install on the B2
 490 floor together with the T2K proton module and the INGRID module as shown in Figure 23.
 491 The proton module is to be used as the entering muon veto and also for the comparison
 492 of interaction between CH and Water. The INGRID module will act as the muon detector
 493 for this period but due to its limited acceptance angle this is only a temporary measure.
 494 The detector was commissioned and since October has been in operation taking data with
 495 the T2K antineutrino beam.

496 The production of the components of the side muon range detectors has been completed
 497 and now the detectors are being assembled at the Yokohama National University. These
 498 detectors will be installed between January and June 2018, when T2K is not running.

499 The Baby MIND detector was transported from CERN to Japan in December, 2017.
 500 It will be installed and commissioned in Jan.-Feb. 2018 and T59 will take the neutrino-
 501 induced muon data in April and May.

502 5 MC studies

503 5.1 Simulation setup

504 The expected number of neutrino events in the water-in Wagasci detector is predicted by
 505 Monte Carlo simulations. Neutrino beam flux at the detector location is simulated by
 506 T2K neutrino flux generator, JNUBEAM. Neutrino interactions with target materials are
 507 simulated by a neutrino interaction simulator, NEUT. Detector responses are simulated
 508 using GEANT4-based simulation.

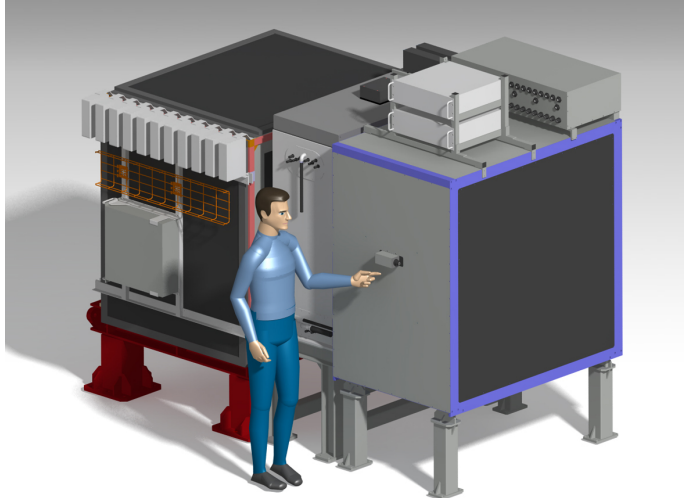


Figure 23: J-PARC T59 detector configuration in October 2017.

509 The detector geometry in the simulation so far is different from the actual setup as
 510 shown in Figure 24. The active neutrino target region consists of four WAGASCI modules.
 511 The size of the WAGASCI module is same as the actual one: 1000 mm × 1000 mm in the
 512 x and y directions and 500 mm along the beam direction (z-direction). Two Side-MRD
 513 modules are installed either side of the Wagasci modules. Each Side-MRD module consists
 514 of ten iron plates whose dimension is 30 mm (thickness) × 2000 mm (height) × 3200 mm
 515 (width). The distance between the Side-MRD modules and WAGASCI modules is 800
 516 mm. The downstream-MRD is equivalent to the Baby-MIND, but without the magnetic
 517 field. It consists of thirty iron plates whose dimension is 30 mm (thickness) × 2000 mm
 518 (height) × 4000 mm (width). The distance between the downstream-MRD modules and
 519 WAGASCI modules is 800 mm. Update of the study with the actual geometry is now
 520 underway.

521 To simulate the signal, the energy deposit inside the scintillator is converted into the
 522 number of photons. The effects of collection and attenuation of the light in the scintillator
 523 and the WLS fiber are simulated, and the MPPC response is also taken into account. The
 524 light yield is smeared according to statistical fluctuations and electrical noise.

525 **5.2 Charged-current event selection**

526 Tracks are reconstructed in two-dimensional planes in each sub-detector. Then, track
 527 matching among the sub-detectors and three-dimensional track reconstruction are per-
 528 formed. These analysis tools have been developed from the software tools by the T2K

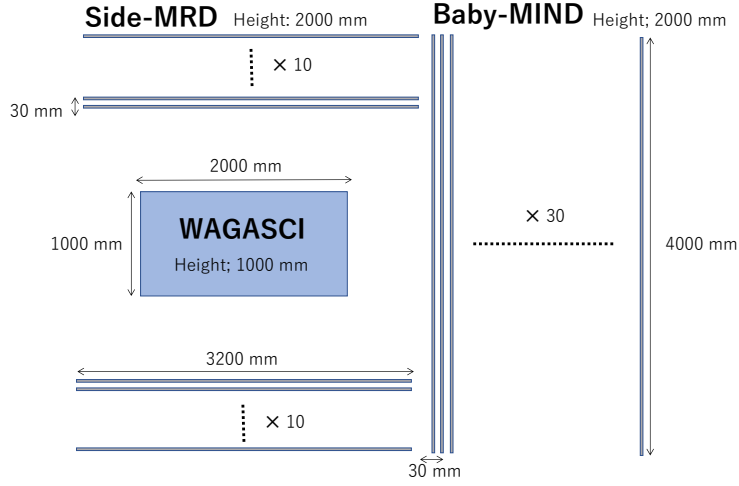


Figure 24: Geometry of the detectors in the Monte Carlo simulation.

529 INGRID and in mature stage already.

530 The events are selected as follows. The starting point of the track is required to be
 531 50 mm away from the edge of the WAGASCI module. This is to remove the background
 532 from the outside. The longest track has to penetrate more than one (five) iron plates in
 533 Side-MRD modules (Baby-MIND). This cut select a muon track and rejects backgrounds
 534 from NC and neutral particles. Then, in order to determine the muon momentum, it is
 535 required that the longest track stops in MRDs (Side-MRD modules and Baby-MIND) or
 536 penetrate all iron plates.

537 Table 1 shows numbers of the selected events in one water-in WAGASCI module after
 538 the event selection. We expect 4,239 (1,666) events from charged-current interaction on
 539 H_2O with 5×10^{20} POT in (anti)neutrino-mode with one water-in WAGASCI module.
 540 The purity, when interactions on CH is counted as background, is 78% for the neutrino-
 541 mode. There is a significant contamination from the wrong-sign (neutrino) interaction for
 542 antineutrino-mode, however, we expect that it will be removed with efficiency higher than
 543 90% by Baby MIND.

544 Table 2 and 3 summarize contributions classified by the interaction types and final state
 545 topologies for the selected charged current-interaction events, respectively.

546 Figure 25 shows the reconstructed angles of the longest tracks in the selected events in
 547 the neutrino-mode and the anti-neutrino mode. Figure ?? shows the iron plane numbers
 548 in Side-MRD and Baby-MIND corresponding to the end points of the longest tracks in the
 549 selected events in the neutrino-mode and the anti-neutrino mode.

Table 1: Expected number of the selected neutrino-candidate events in one water-in WAGASCI module with 5×10^{20} POT in each of neutrino-mode and antineutrino-mode. Note that the wrong sign component will be reduced by one order by applying the charge selection by Baby MIND.

| | CC on H ₂ O | NC on H ₂ O | Interaction on CH | wrong sign interaction |
|-------------------|------------------------|------------------------|-------------------|------------------------|
| ν -mode | 4239 | 107 | 1087 | (negligible) |
| anti- ν -mode | 1666 | 14 | 560 | (561) |

Table 2: Interaction types for the selected charged-current events.

| | CCQE | 2p2h | CC resonant π | CC-DIS |
|-------------------|--------|-------|-------------------|--------|
| ν -mode | 48.4 % | 9.7 % | 27.1 % | 14.7 % |
| anti- ν -mode | 57.1 % | 8.2 % | 17.3 % | 17.3 % |

Table 3: Final state topologies for the selected charged-current events.

| | CC0 π | CC1 π | CC2 π | CCn π |
|-------------------|-----------|-----------|-----------|-----------|
| ν -mode | 67.4 % | 20.9 % | 3.0 % | 8.7 % |
| anti- ν -mode | 79.5 % | 16.3 % | 1.2 % | 3.0 % |

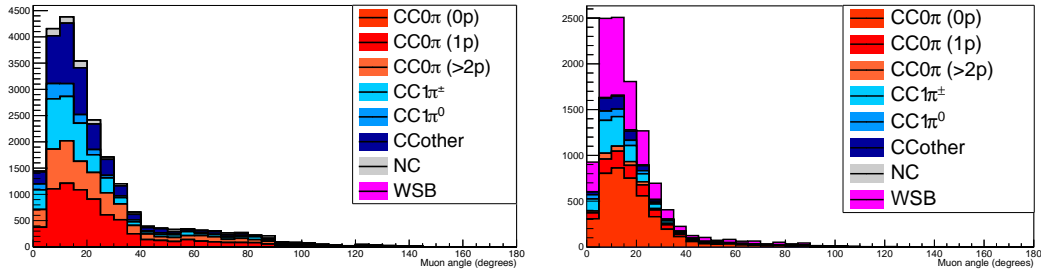


Figure 25: The reconstructed angles of the longest tracks in the selected events in the neutrino-mode (left) and the antineutrino-mode (right).

550 5.3 Standalone WAGASCI-module tracking performance

551 The previous section has described the inclusive charged-current event selection using the
 552 Muon Range detectors. A muon is identified by requiring one track to penetrate multiple
 553 planes of the MRD's. For the WAGASCI configuration described in Sec. 5.1, only 7% of
 554 the muons are stopped in one of the WAGASCI modules. This proportion increases to
 555 53% for pions and 73% for protons produced by neutrino interactions. Figure 27 shows the
 556 momentum distribution of these daughter particles as well as for the sub-sample stopped
 557 in one of the WAGASCI modules. For the measurement of the neutrino interaction final
 558 states, tracks of charged pions, protons and low-momentum ($p_\mu < 300$ MeV/c) muons have
 559 to be reconstructed by the WAGASCI module. Therefore, the standalone tracking abilities
 560 of the WAGASCI module, especially momentum threshold, is important for the exclusive
 561 interaction measurements.

562 Here we present the result of the study based on an original study done for the T2K
 563 ND280 upgrade with some modifications. Though the cell size is similar to the WAGASCI
 564 configuration, the external dimensions are different (1864 mm \times 600 mm \times 1300 mm). We
 565 present the results which are less affected by the difference of the external dimensions.

566 A simplified criteria , but representing conditions for the WAGASCI module tracking,
 567 are applied to evaluate the reconstruction performance of the WAGASCI module. The
 568 fiducial volume is chosen as the inner cube of the module which surfaces are 4 \times scintillator
 569 space = 100 mm distant from the module external surfaces. A track is reconstructed if:

- 570 • The track is long enough and has at least 2 hits in both of two views (XZ, YZ). In
 571 the pure longitudinal or transverse going tracks, it corresponds to the track length
 572 of 100 mm.
- 573 • The track shall not be superimposed with longer tracks in both of two views. The
 574 superposition criterion is estimated with the distance inter-tracks (DIT) which cor-
 575 responds to the orthogonal distance between two tracks at the ending point of the

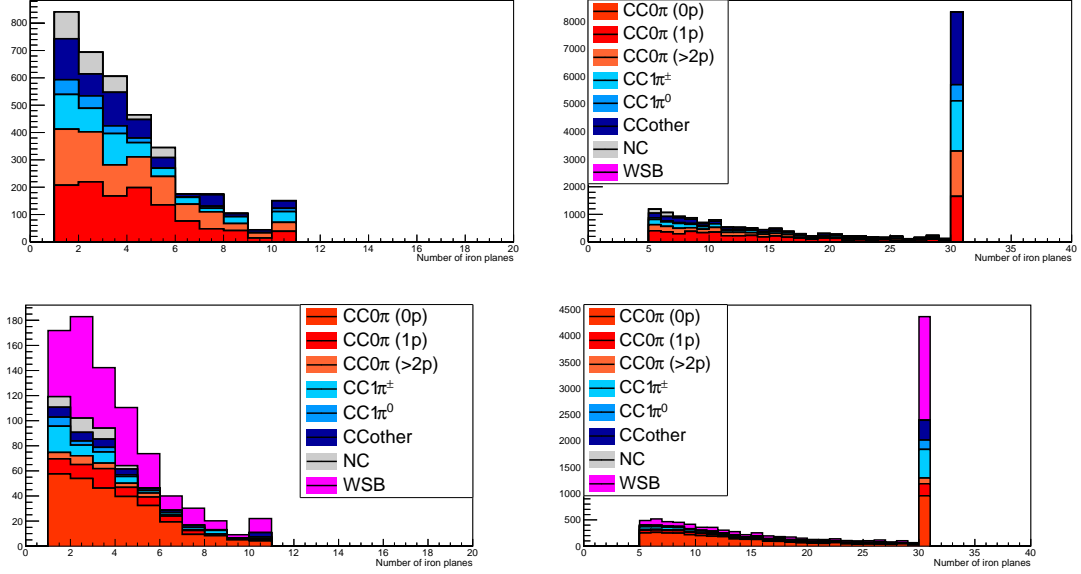


Figure 26: Iron plane numbers in Side-MRD (left) and Baby-MIND (right) corresponding to the end points of the longest tracks in the selected events in the neutrino-mode (top) and the antineutrino-mode (bottom).

576 shortest one (see Figure 28). The DIT should be higher than $4 \times$ scintillator width
577 ($=100$ mm) for the shorter track not to be superimposed with the longer track.

578 5.3.1 Expected performance of the water-in WAGASCI module

579 Figures 29 shows the expected track reconstruction efficiency obtained with the criteria
580 above. Table 4 summarizes the reconstruction efficiencies and the reconstruction momen-
581 tumbum thresholds. This threshold is defined as the momentum under which the reconstruction
efficiency falls under 30%. The thresholds for muon and pion are 150 MeV/c. The lower

Table 4: Reconstruction efficiency and momentum threshold for muons, pions and protons.
The threshold is defined as the momentum under which the reconstruction efficiency falls
under 30%.

| | μ | π | p |
|---------------------------|-----------|-----------|-----------|
| Reconstruction Efficiency | 79% | 52% | 26% |
| Momentum threshold | 150 MeV/c | 150 MeV/c | 550 MeV/c |

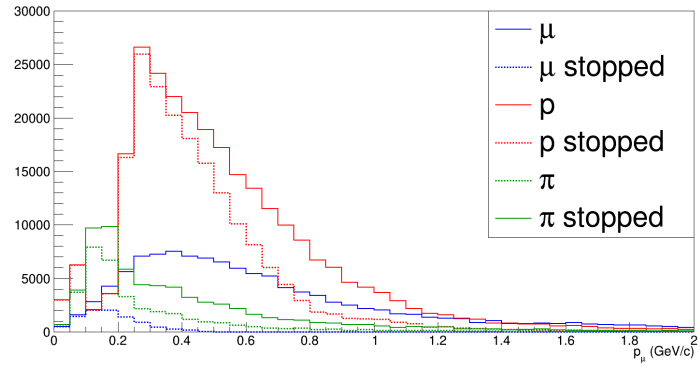


Figure 27: Momentum distribution of particles in WAGASCI (plain) and corresponding distributions only for particles stopping in the WAGASCI module (dashed).

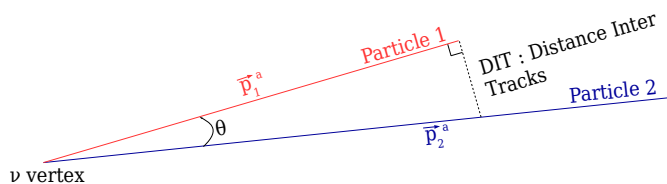


Figure 28: Definition of the distance inter tracks.

582 pion and proton efficiencies (respectively 52% and 26%) are due to lower momentum and
 583 also due to the secondary interaction. Efficiencies of each particle type tend to decrease in
 584 the backward region due to lower particle momenta. However, for a fixed momentum value,
 585 the reconstruction efficiency do not strongly depend on the angle thanks to the WAGASCI
 grid structure.

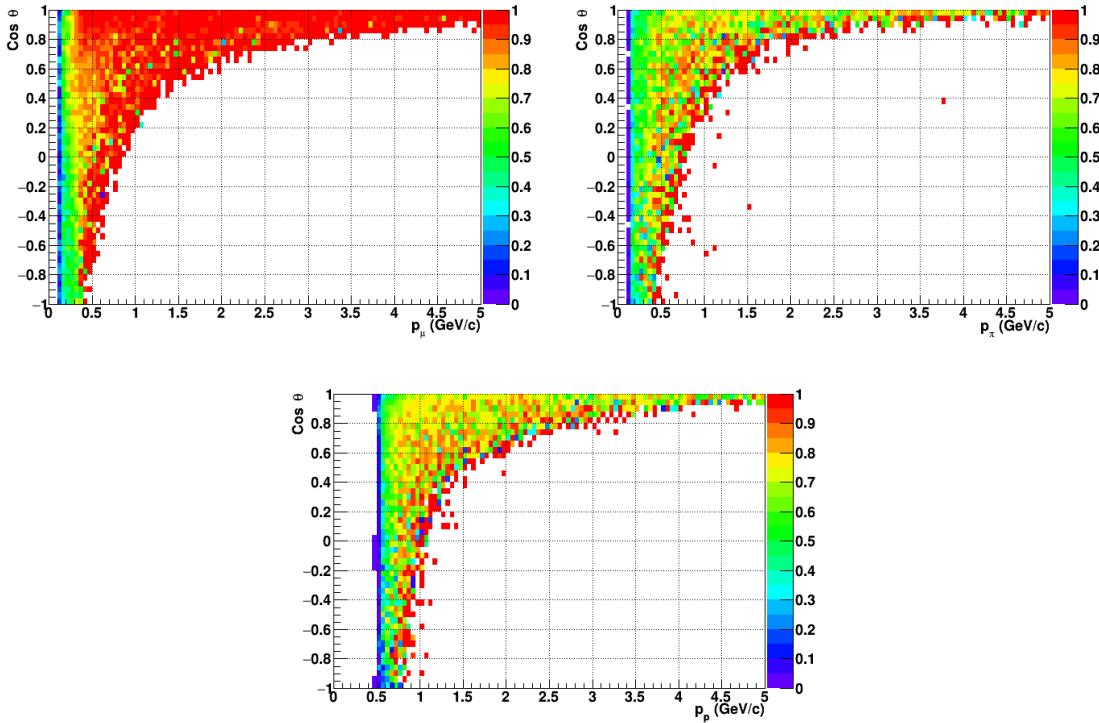


Figure 29: Reconstruction efficiency of muons (left), charged pions (right) and protons (bottom) in the WAGASCI water-module as a function of the particles momenta and angles.

586

587 5.3.2 Expected performance of the water-out WAGASCI module

588 One experimental option is to remove water from one of the two WAGASCI modules. The
 589 detector is fully active and has a 3 mm spatial resolution (scintillator thickness) which
 590 create an ideal detector to reconstruct and identify hadrons, and study 2p2h interaction.
 591 The same reconstruction criteria as in Sec. 5.3.1 are applied for the water-out module.
 592 Figure 30 shows the comparison between the water-in and the water-out reconstruction
 593 efficiencies for muon, pions and protons. 90% of the muons and 87% of the pions are
 594 reconstructed, while 70% of the protons are even reconstructed. It allows to low down the

proton threshold to 250 MeV/c (see Table 5). The water-out module offers interesting

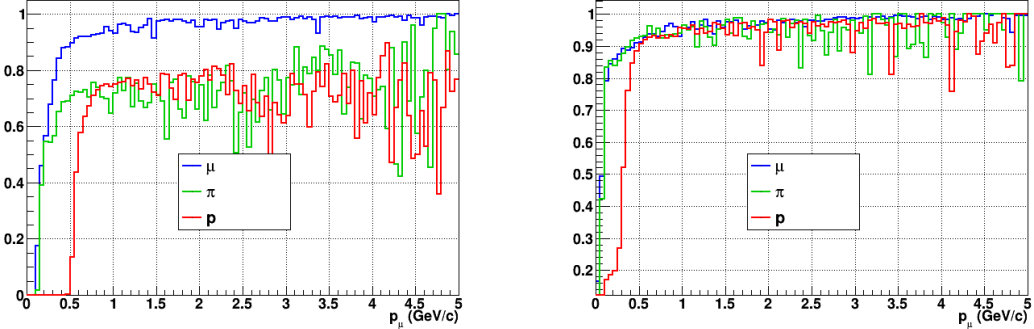


Figure 30: Reconstruction efficiency for muons, pions and protons in the water-in (left) and water-out (right) modules.

Table 5: Reconstruction efficiency, proportions of μ -like and non μ -like and momentum threshold for muons, pions and protons for the water-out module. The threshold is defined as the momentum under which the reconstruction efficiency falls under 30%.

| | μ | π | p |
|---------------------------|----------|----------|-----------|
| Reconstruction Efficiency | 90% | 87% | 70% |
| Momentum threshold | 50 MeV/c | 50 MeV/c | 250 MeV/c |

595

596 possibilities to study 2p2h interaction since 70% of the protons are reconstructed.

597

6 Schedule

598

599 We would like to start physics data-taking with T2K beam after the summer shutdown in
600 to be complete. The experiment can run parasitically with T2K, therefore we request no
601 dedicated beam time nor beam conditions as discussed in the following section.

602

7 Requests

603

7.1 Neutrino beam

604

605 The experiment can run parasitically with T2K, therefore we request no dedicated beam
time nor beam condition. T2K has been requesting 0.9×10^{21} POT/year and actually

606 accumulating about 0.7×10^{21} POT/year in recent years. For each year, starting from the
607 Autumn, T2K is running predominantly in the neutrino mode or in the antineutrino mode.
608 Our request is to have one-year neutrino-mode data and another one-year antineutrino
609 mode data assuming that the POT for the fast extraction in each year is more than $0.5 \times$
610 10^{21} POT.

611 7.2 Equipment request including power line

612 We request the following in terms of equipment on the B2 floor:

- 613 • Site for the WAGASCI modules, Side-MRD modules and BabyMIND and their elec-
614 tronics system on the B2 floor of the near detector hall (Figure 2 and 3).
- 615 • Anchor points (holes) on the B2 floor to secure the WAGASCI modules, Side-MRD
616 module and Baby-MIND. Detailed floor plans to be communicated in a separate
617 document.
- 618 • Power line for the magnets in Baby-MIND: 400 V tri-phase 48-to-62 Hz, capable of
619 delivering 12 kW. We request the magnet power line to be installed and available to
620 us by beginning of March 2018.
- 621 • Electricity for electronics and water circulation system. We request a total of 3 kW
622 of power in standard Japanese electrical sockets for the following items:
 - 623 1. Online PCs: 2.1 kW
 - 624 2. Electronics: 0.7 kW
 - 625 3. Water sensors: 1 kW
- 626 • Air conditioner for cooling heat generation at Baby-MIND magnets, online PCs and
627 electronics
- 628 • Beam timing signal and spill information
- 629 • Network connection

630 The infrastructure for much of the above exists already. Exceptions are the power line
631 for the magnet and the electronics and holes in the B2 floor to anchor the detector support
632 structures.

633 After this WAGASCI experiment, Baby MIND and Side-MRD's will remain if approved
634 by J-PARC, and be used as common platforms of future neutrino experiments using the
635 J-PARC neutrino beam.

636 **References**

- 637 [1] K. Abe et al. Measurement of the muon neutrino inclusive charged-current cross
638 section in the energy range of 13 GeV with the T2K INGRID detector. *Phys. Rev.*,
639 D93(7):072002, 2016.
- 640 [2] K. Abe et al. Measurement of neutrino and antineutrino oscillations by the T2K
641 experiment including a new additional sample of ν_e interactions at the far detector.
642 *Phys. Rev.*, D96(9):092006, 2017.
- 643 [3] M. Antonova et al. Baby MIND Experiment Construction Status. In *Prospects in*
644 *Neutrino Physics (NuPhys2016) London, London, United Kingdom, December 12-14,*
645 *2016*, 2017.
- 646 [4] K. Nitta et al. The k2k scibar detector. *Nucl. Instrum. Meth. A*, 535:147, 2004.
- 647 [5] K. Abe et al. (T2K Collaboration). Measurement of the inclusive ν_μ charged current
648 cross section on iron and hydrocarbon in the t2k on-axis neutrino beam. *Phys. Rev.*
649 *D*, 90:052010, 2014.
- 650 [6] F. Magniette F. Gastaldi, R. Cornat and V. Boudry. A scalable gigabit data acquisition
651 system for calorimeters for linear collider. *proceedings of TIPP2014*, page PoS 193,
652 2014.
- 653 [7] J. Fleury, S. Callier, C. de La Taille, N. Seguin, D. Thienpont, F. Dulucq, S. Ahmad,
654 and G. Martin. Petiroc and Citiroc: front-end ASICs for SiPM read-out and ToF
655 applications. *JINST*, 9:C01049, 2014.
- 656 [8] M. B. Barbaro J. A. Caballero T. W. Donnelly G. D. Megias, J. E. Amaro. Inclusive
657 electron scattering within the susav2 meson-exchange current approach. *Phys. Rev.*
658 *D*, 94:013012, 2016.
- 659 [9] M. Valverde J. Nieves, J. E. Amaro. Inclusive quasi-elastic neutrino reactions. *Phys.*
660 *Rev. C*, 70:055503, 2004.
- 661 [10] Yu. G. Kudenko, L. S. Littenberg, V. A. Mayatsky, O. V. Mineev, and N. V. Ershov.
662 Extruded plastic counters with WLS fiber readout. *Nucl. Instrum. Meth.*, A469:340–
663 346, 2001.
- 664 [11] O. Mineev, Yu. Kudenko, Yu. Musienko, I. Polyansky, and N. Yershov. Scintillator
665 detectors with long WLS fibers and multi-pixel photodiodes. *JINST*, 6:P12004, 2011.
- 666 [12] Etam Noah et al. Readout scheme for the Baby-MIND detector. *PoS*, Photo-
667 toDet2015:031, 2016.
- 668 [13] Omega. Spiroc 2 user guide. 2009.